Vacuum 154 (2018) 52–57

Contents lists available at ScienceDirect

Vacuum

journal homepage: www.elsevier.com/locate/vacuum

Influence of the oxygen consumption on the crystalline structure of titanium oxides thin films prepared by DC reactive magnetron sputtering

Roberto Villarroel[a], Rodrigo Espinoza-González[a,*], Judit Lisoni[b], Guillermo González-Moraga[c]

[a] LabMAM, Depto. de Ingeniería Química, Biotecnología y Materiales, Av. Beauchef 851, Santiago, Chile
[b] Instituto de Ciencias Físicas y Matemáticas, Facultad de Ciencias, Universidad Austral de Chile, Valdivia, Chile
[c] Departamento de Química, Facultad de Ciencias, Universidad de Chile, Santiago, Chile

ARTICLE INFO

Keywords:
Reactive sputtering
Film pumping speed
Titanium suboxides

ABSTRACT

In the present work, a simple route to control the growth of different crystalline titanium oxides thin films prepared by reactive sputtering is reported. Using the film pumping speed, the oxygen consumption or "oxygen gettering" in the reactive process is monitored, obtaining different titanium suboxides (TSO's) films with high deposition rate in the metallic zone of the reactive process. On the other hand, it was also obtained titanium dioxide (TiO_2) thin films at the beginning of the oxidative region, without using postdeposition thermal annealing. X-ray diffraction and Raman spectroscopy were used to determine the different titanium oxides according to the oxygen percentage added to the chamber during the reactive process.

1. Introduction

Titanium oxides are one of the most studied materials over the past decades. The most common oxide is the IV valence titanium dioxide, TiO_2. There are many different uses for this semiconductor such as white paints and coatings [1], pharmaceutical and cosmetics industries [2], photocatalytic degradation (mineralization) of pollutants [3], energy production by water splitting [4] or photoelectrochemical solar cells [5], antireflective [6] and UV induced self-cleaning [7] coatings. TiO_2 has three crystalline phases: anatase, rutile and brookite. The most common ones are rutile and anatase, which are tetragonal (space groups $I4_1/amd$ and $P4_2/mnm$, respectively), while brookite is orthorhombic (Pbca) [8].

In the last years, the study of different non-stoichiometric titanium suboxides (TSO's) has attracted attention due to the high electrical conductivity [9], remarkable visible light absorption [10] and electrochemical corrosion resistance [11]. These properties have made TSO's potential candidates for various applications such as catalysts [12] and battery electrodes [13] as well as for micro and optoelectronic devices [14]. Among different TSO's, TiO and Ti_2O_3 are of great interest. Titanium monoxide (TiO) has a NaCl-type cubic structure and a composition that ranges from $TiO_{0.6}$ to $TiO_{1.25}$ [15]. Due to the low electrical resistivity of TiO, it has potential uses in microelectronics devices [16–18] and it is a promising compound for new thermoelectric materials [19]. Ti_2O_3 is a corundum-type rhombohedral structure with a non-stoichiometric range from $TiO_{1.49}$ to $TiO_{1.51}$ [15]; it is a semiconductor with a direct band gap of ~0.1 eV. The most remarkable property of Ti_2O_3 is the metal-to-semiconductor transition at 400 K, close to room temperature, without a change in crystal symmetry [20,21].

TSO's are mainly prepared by reduction processes of TiO_2, such as carbothermic reduction [22], hydrogen reduction [23], and metallothermic reduction [24]. Reactive sputtering is a common technique to growth thin film compounds with high control of the stoichiometry. Several approaches have been done theoretically and experimentally to explain the metal-oxygen interaction during the reactive process and the relevant sputtering parameters involved in the reactions [25–30]. For titanium oxides, the investigations are mainly related to obtain the specific TiO_2 polymorph, working in the oxidized or transition zone of the reactive process. Substrate temperature [31], partial pressure of oxygen [32–34], bias voltage and energy of the impinging ions [35,36] have been reported as the main influencing parameters to control the growth of mixed or single rutile/anatase phases. Regarding the TSO's, studies based upon the oxygen partial pressure have mainly demonstrated that there is a direct transition between TiO in the metallic zone of the reactive process, to TiO_2 in the oxidized zone [37–40].

This work presents the results of the relation between the oxygen consumption and the growth of different titanium oxides, deposited by DC reactive sputtering. The structural properties of the grown films in the Ti-O system were obtained by X-Ray diffraction and Raman spectroscopy. Meanwhile, details about the morphological evolution were obtained by Field-emission scanning electron microscopy and atomic

* Corresponding author.
E-mail address: roespino@ing.uchile.cl (R. Espinoza-González).

https://doi.org/10.1016/j.vacuum.2018.04.049
Received 3 February 2018; Received in revised form 27 April 2018; Accepted 28 April 2018
Available online 30 April 2018
0042-207X/ © 2018 Elsevier Ltd. All rights reserved.

Table 1
Oxygen flow percentages (OP) employed for sample preparation and, the representative colors, thickness and deposition rates of the different of the Ti-oxide film samples.

Sample	Oxygen flow percentage	Color	Thickness (μm)	Deposition rate (nm/min)
Silv	4.6%	Silver	2.83	94
Gol-1	6.1%	Golden	3.12	104
Gol-2	7.4%	Golden	3.21	107
Gol-3	8.9%	Golden	3.62	121
Black	11.1%	Blackish	3.50	117
Tran-1	12.7%	Transparent	0.73	12
Tran-2	14.2%	Transparent	0.50	8

force microscopy.

2. Experimental procedure

The films were grown by DC magnetron sputtering. A titanium disk of 2″ diameter and 0.25″ thickness (Kurt Lesker 99.99%) was used as target material. The base pressure in the vacuum system was 5×10^{-6} Torr, and the target-to-substrate distance was 45 mm for all samples. Based upon preliminary experiments, the optimal growth conditions for crystalline titanium oxides were obtained at 150 W (7.4 W/cm^2), corresponding to a working pressure of 5×10^{-3} Torr. This working pressure was attained using different combinations of Ar + O_2 in a total flux of 15 sccm. In the following, the oxygen quantity used for the growth of the different films is represented by the oxygen flow percentage (OP) of the total gas flux injected into the chamber. Table 1 shows the conditions used in this work, selected according to the variation of the curve of oxygen integration, as it will be discussed later in detail. The deposition time was 30 min for the films with OP < 12% and 60 min for the films with OP ≥ 12%. The conditioning of the target prior to deposition was done by 20 min of sputtering in pure Ar-gas at 5×10^{-3} Torr. Finally, for the plasma stability, the current and voltage during sputtering were monitored.

The grain structure of the films was studied using a field emission scanning electron microscope (FESEM) FEI Quanta 250 system. The characterization of the surface topography of the films was done by atomic force microscopy (AFM) using a NT-MDT NTegra Prima in Semicontact configuration. The crystalline phases were characterized by X-ray diffraction (XRD) in a Bruker D8 diffractometer using CuKα radiation. The data were collected at room temperature with a step size of 0.02° and a scan rate of 0.1°/s using the Bragg-Brentano geometry (or coupled-scan). The lattice parameters were calculated using the indexation provided by the identified Powder Diffraction Files for each structure. The crystallite size (*CS*) was obtained by Scherrer equation [41]. Raman spectra were obtained using a Witec Alpha 300 RA with backscattering geometry and excitation wavelength of 532 nm.

3. Results and discussions

3.1. Determination of the oxygen consumption during the reactive process

Pinnow et al. [42] proposed to monitor the reactive sputtering process considering the oxygen consumption or oxygen "gettering" that occurs as a consequence of the integration of the reactive gas with the metal. They used the film pumping speed as a control parameter, developing a generic curve determined by a sputtering equilibrium, which depends on the oxygen partial pressure, the sputtering power, and the pumping speed of the vacuum system. The parameter *film pumping speed, s_f,* was defined as the consumption of the reactive gas after the plasma ignition and can be related to the variations of the oxide phase during the deposition of metallic oxides by reactive sputtering. Based on this they could optimized the sputtering process setting the working point to obtain an adequate stoichiometry and higher deposition rates for IrO_x and IrO_2 films [42].

In order to determine this parameter, it is necessary to define the change in the total pressure inside the chamber that can be described as:

$$\frac{dP}{dt} = \frac{1}{V}(Q_{in} + Q_{des} - Q_{ads} - P_{(t)} \cdot s_p) \quad (1)$$

where Q_{in} is the total gas flow entering to the chamber ($Q_{Ar} + Q_{O_2}$), s_p is the system pumping speed, Q_{des} and Q_{ads} are the total fluxes adsorbed or desorbed by the target and chamber walls and, P is the total pressure of the system. After the system has reached equilibrium, $dP/dt = 0$, it is assumed the balance between adsorbed and desorbed gases by the chamber walls and the target. Hence, the total gas flow in equilibrium can be represented as:

$$Q_{in} = P_0 \cdot s_p \quad (2)$$

where P_0 is the working pressure mentioned above. After plasma ignition, the film growth consumes reactive gas, changing the total pressure inside the chamber. Consequently, Eq. (2) can be rewritten as:

$$Q_{in} = P_{sp} \cdot (s_p + s_f) \quad (3)$$

where P_{sp} represents the total pressure after plasma ignition and, s_f is the film pumping speed produced by oxygen consumed during film formation. The film pumping speed, s_f, can be deduced from the combination of Eq. (2) and Eq. (3) as follows:

$$s_f = \frac{s_p}{P_{sp}}(P_0 - P_{sp}) \quad (4)$$

Thus, based on the results of Pinnow et al. [42], in this work it was studied the variations of the film pumping speed in the Ti-O system. The values of s_f were obtained at different oxygen percentages of the total flow inside the chamber (OP %), which results are plotted in Fig. 1. It can be seen that s_f increases until it reaches a maximum value at OP = 11.1%. Afterwards, it decreases to almost 0 (OP = 14.2%), or below the detection limit of the instruments, with a slight plateau between 7.4 and 8.9%. The drastic drop down of s_f at higher OPs corresponds to a saturation behavior, in which the oxygen consumption reaches its maximum and oxygen starts to be adsorbed on the titanium target surface. At high oxygen flows, the target becomes oxidized or "poisoned" thus changing the plasma and consequently the deposition conditions significantly. This zone is called as "saturated regime" in the further discussion, while the zone corresponding to the metallic behavior of the target is named as "unsaturated regime" of the reactive

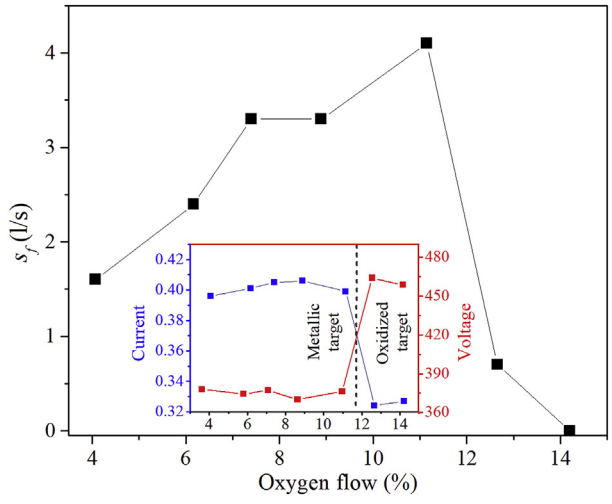

Fig. 1. Film pumping speed, s_f, versus oxygen flow percentage. Insert: Current and voltage of the magnetron source during sputtering.

plasma deposition.

Simultaneously to the measurements of s_f, the voltage and current were monitored after plasma ignition, as a function of OP (inset in Fig. 1). The plasma voltage is almost constant until OP reaches 11.1%. Afterwards, a drastic increase can be observed. The current increases until a maximum at OP = 8.9% and after a slight decrease it falls suddenly, which correlates well with the significant increase in voltage. This phenomenon also confirms the changes in the target surface composition from a metallic behavior at low OP to an oxidized and less conductive behavior at high OP.

Therefore, it is of interest to understand the phenomenon of oxygen being gettered by the film before saturation. During reactive sputtering, the OP range of the metallic regime strongly depends on the power used for the ignition of the plasma as shown by Pinnow et al. [42]. For lower powers, the saturation is reached with less amount of oxygen while increasing the power allows to extend the OP range of the metallic regime. In this work, using a power of 150 W, the metallic zone of the reactive process can be extended to an OP of 11%.

The growth of Ti-oxide was carried out using the OP conditions reported in Table 1. The first evident observation is that the samples exhibited different colors (Table 1), which varied from silver (Silv) to golden in samples Gol-1, Gol-2 and Gol-3 (OP between 6.1 and 8.9%). The highest s_f obtained at an OP = 11.1% produced a blackish color in sample Black. Finally, when s_f decreased suddenly the samples Tran-1 and Tran-2 were transparent (OP = 12.7 and 14.2%).

3.2. Microscopy analysis

3.2.1. Field emission scanning electron microscopy (FESEM)

Cross-section FESEM images of the thin films prepared at different OPs are presented in Fig. 2. It can be seen that the films thickness reaches values of nearly 3 μm (Table 1) for samples deposited in the unsaturated regime of s_f, while in the saturated regime (Tran-1 and Tran-2) the films are sub-micrometer with values of 730 and 500 nm, respectively. These smaller film thicknesses are related with the target poisoning that strongly reduces the sputter yield in this stage. Based upon the thickness and deposition times, it is possible to estimate the deposition rate for each OP, which are given in Table 1. The low sputtering rate of the thin films in the unsaturated regime confirms that a reduced s_f is related to target poisoning.

The relation between the deposition rate and the OP demonstrates a typical behavior of Ti-O systems studied by reactive sputtering, in which the deposition rate strongly decreases as the target poisoning starts [43]. The deposition rate increases with OP until it reaches a maximum at an OP of 8.9% (sample Gol-3) that slightly decreases in Black sample. In the saturated stage, the low deposition rate also leads to films with a granular structure and randomly disorder columnar grains, as it can be seen in Fig. 2f and g for samples Black and Tran-2, respectively.

3.2.2. Atomic force microscopy (AFM)

AFM measurements were carried out to characterize the surface of the Ti-oxide films. Representative AFM images of the films are shown in Fig. 3, while the root mean square roughness (RMS) is given in Table 2. The surface morphology and roughness changes significantly as a function of the OP. RMS has an increasing tendency with OP until it reaches a maximum at OP = 8.9%. In the saturated regime, transparent samples Tran-1 (not shown in Fig. 3) and Tran-2 also have smooth surfaces with RMS values of 6.5 and 4.1, respectively.

3.3. Crystalline phase analysis

3.3.1. XRD characterization

Fig. 4 shows the X-ray diffraction patterns for samples deposited at different OPs. An evolution of the patterns according to the oxygen gettered in the reactive process during the film deposition can be seen. The crystalline structures identified in each pattern and their corresponding lattice parameters are summarized in Table 2. Silv sample shows the hexagonal structure of α-Ti (JCPDS 76–1644), which is a Ti-rich phase with a structure close to that of hcp titanium. In this

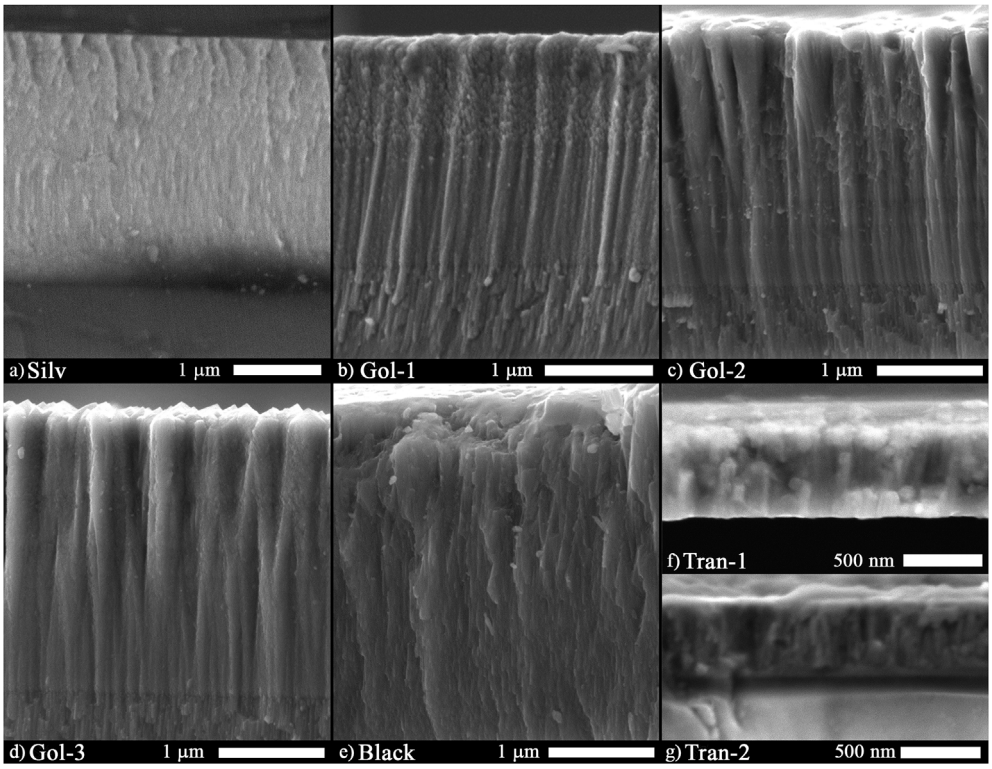

Fig. 2. FESEM images of the Ti-oxides thin films prepared at different OP.

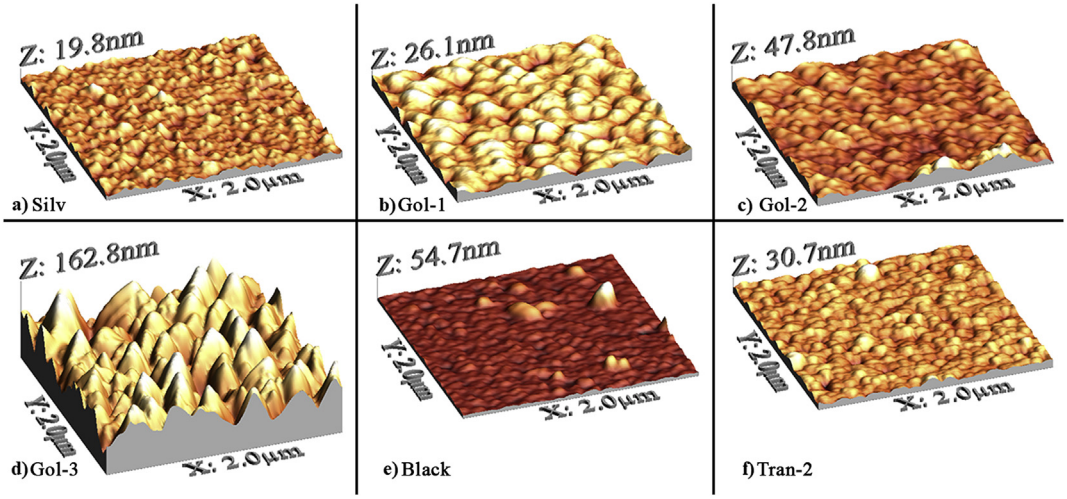

Fig. 3. AFM images of the Ti-oxides thin films prepared at different OPs.

Table 2
Summary of the surface roughness (RMS) measured by AFM and the results obtained from the XRD patterns.

Sample	RMS (nm)	Phase	Crystallographic system	Crystallite size, *CS* (nm)	Lattice parameter (nm)	
					a	c
Silv	2.2	Ti_3O	Hexagonal	6	0.516	1.401
Gol-1	3.8	TiO-type	Cubic	26	0.417	–
Gol-2	5.2	TiO-type	Cubic	28	(1)	–
Gol-3	23.4	TiO-type	Cubic	17		–
Black	3.9	Ti_2O_3-type	Rhombohedral	16	0.514	0.137
Tran-1	6.5	TiO_2	Tetragonal	(A) 47	0.378	0.946
				(R) 14	0.460	
Tran-2	4.1	TiO_2	Tetragonal	(A) 43	0.378	0.946
				(R) 14	0.460	

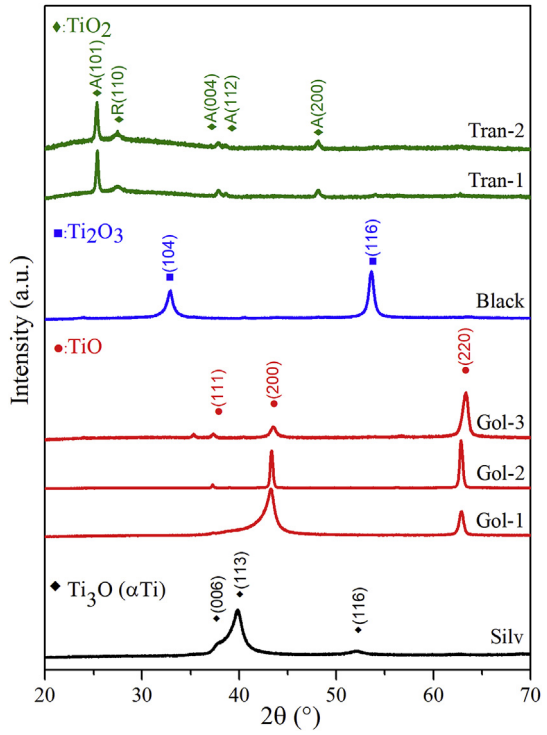

Fig. 4. X-Ray diffraction pattern of the titanium oxide films deposited at different OP. A: Anatase; R: Rutile.

crystalline structure, oxygen atoms are partially dissolved in octahedral interstices [44] forming an oxide, which known as Ti_3O. For the samples Gol-1, Gol-2 and Gol-3 only the TiO-type cubic structure (JCPDS 89–5010) was detected in the OP range from 6.0 to 8.9%. Particularly, the lattice parameter of the TiO phase decreases as the OP increases. This is in good agreement with the observations of Anderson et al. [15] who demonstrated that the TiO phase can stabilize the same crystalline structure with a wide range of O-content. The pattern of sample Black exhibited a Ti_2O_3-like structure (JCPDS 89–4746). Interestingly, Ti_2O_3 is obtained at the OP that corresponds to the maximum value of s_f. Regarding the samples Tran-1 and Tran-2 prepared in the saturated regime, XRD patterns were indexed with anatase (JCPDS 21–1272) and rutile (JCPDS 21–1276) TiO_2 phases, respectively. As a general observation of the XRD characterization, it can be deduced that as the OP increases, the O/Ti ratio increases as well thus forming zones of specific oxide growth. As a consequence, the color of the films correlates well with a specific crystalline structure and oxide species. The silver zone represents the preferred growth of the α-Ti structure, the golden zone shows the growth of TiO structure, the narrowed blackish zone represents Ti_2O_3 growth and the transparent zone corresponds to the growth of the two TiO_2 polymorph, i.e. anatase and rutile.

The crystallite sizes, *CS*, estimated by Scherrer's equation are listed in Table 2. It can be seen that the values vary with the crystallographic system of the Ti-oxide. It can be assumed that there is a relationship between the RMS of the samples surface, the color of the samples and the crystalline structure. Indeed, the silver sample has the lowest RMS and the lowest *CS*, while the golden samples (Gol-1 and Gol-2) have a columnar growth structure (see Fig. 2) with slightly increased values for RMS and *CS*. Sample Gol-3 can be considered as an exception, since it displays rather a large value for RMS combined a low value for CS. This behavior of Gol-3 may be related to an increment of the substrate temperature during film deposition [45] as inferred from the maximum current measured during plasma ignition. A higher current implies more electrons and thus a higher plasma density. In sample Black, the change of the crystalline structure coincides with a smaller RMS and lower *CS*. Finally, transparent samples Tran-1 and Tran-2 having granular grains (see Fig. 2f and g) demonstrate low roughness and similar *CS*. These samples further support the observation that the temperature during sputtering is clearly linked to the current measured which is in good agreement with the model presented by Thornton [45].

3.3.2. *Raman spectroscopy*

Raman spectroscopy was performed to study the vibrational response of the films prepared at different OPs. According to the selection

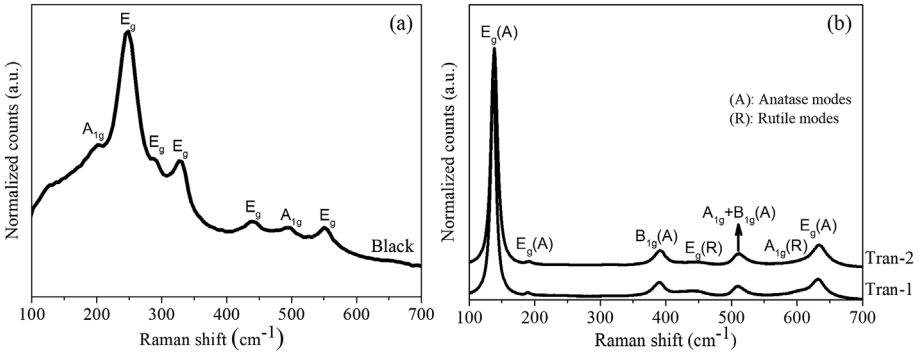

Fig. 5. Raman spectra of samples a) Black and; b) Tran-1 and Tran-2.

Table 3
Details of Raman response for samples Black, Tran-1 and Tran-2.

Sample	Ti_2O_3-like structure			Sample		TiO_2	
Black	[47]	[48]	Symmetry	Tran-1	Tran-2	[49]	Symmetry
Wavenumber (cm^{-1})				Wavenumber (cm^{-1})			
207	–	209.7	A_{1g}	143	144	144	E_g (A)
252	240	274	E_g	195	196	198	E_g (A)
300	288	300	E_g	396	396	397	B_{1g} (A)
340	322	340	E_g	450	453	449	E_g (R)
446	426	453	E_g	515	516	516	A_{1g} + B_{1g} (A)
503	490	506	A_{1g}	611	–	610	A_{1g} (R)
565	552	558	E_g	638	638	639	E_g (A)

rules, α-Ti, and TiO do not have an active first order vibrational mode [46]. Therefore, no Raman spectra can be obtained for samples Silv, Gol-1, Gol-2 and Gol-3. The Raman spectra of the samples Black, Tran-1 and Tran-2 are presented in Fig. 5. The sample Black shown in Fig. 5a has characteristic peaks of five bending modes (E_g) and two stretching modes (A_{1g}), all matching well results of previous works based upon tistarite, a Ti_2O_3 mineral recently discovered in the Allende Meteorite [47], and the synthetic Ti_2O_3 [48]. The details of the peaks position are shown in Table 3. This result confirms the Ti_2O_3-like phase detected by XRD.

The vibrational modes of two different TiO_2 polymorphs - anatase (A) and rutile (R) - were observed in the Raman spectra of samples Tran-1 and Tran-2, as shown in Fig. 5b. This matches well with the presented XRD-results. The Castrejon-Sanchez relation was used to estimate the phase content (W_A/W_R) in these samples [50]:

$$\frac{W_A}{W_R} = 1.01\left[\frac{B_{1g}(A)_{399}}{E_g(R)_{447}} - 0.33\right] \quad (5)$$

where W_A/W_R are the weight ratios of anatase and rutile, respectively. B_{1g} is the intensity of the symmetric stretching mode of the anatase at ~399 cm^{-1}, whereas E_g is the intensity of the symmetric stretching mode of rutile phase at ~447 cm^{-1}. According to Eq. (5), the estimated weight percent of the anatase phase in Tran-1 and Tran-2 are 65 and 76%, respectively. Consequently, the sample Tran-2 shows a higher amount of anatase compared to sample Tran-1. This may be related to the amount of oxygen in the film growth at room temperature as it has been previously reported by other authors [33,51].

4. Discussion and summary

In this work, using the parameter s_f, it was possible to monitor the relation between the oxygen consumption and the growth of different titanium suboxides during reactive sputtering. This parameter mainly depends of the percentage of oxygen present in the chamber and the power used to ignite the plasma.

Based upon the presented results, the growth of three TSO's with different crystalline structure and grain morphology was obtained in the metallic regime of the reactive process, which in turns is reflected by the color, roughness and crystallite sizes of the samples. Specifically, at the beginning of the oxygen integration the hexagonal Ti_3O (α-Ti) structure was obtained. Afterwards, a second stage of crystallization was observed with the formation of the TiO cubic structure. This TiO_x structure was obtained for a wide range of OPs, which was attributed to the wide stoichiometry range of this phase ($0.6 < x < 1.25$). At the end of the metallic regime, a third stage appeared when the oxygen integration reached the maximum value thus forming rhombohedral Ti_2O_3 structure. This narrower OP range can be attributed to the non-stoichiometric range of this phase ($1.49 < x < 1.51$).

Lastly, the oxidative regime of the reactive process induces the growth of mixed rutile and anatase phases of TiO_2. It can be concluded that the higher the OP is, the larger the amount of anatase is, which is a good agreement with observations published by Refs. [33,51].

It is remarkable that all Ti-oxide thin films prepared are crystalline without any post annealing process. Finally, the results presented in this work are important since they can be considered as a stepping stone to extend the potential technological applications of TSO's towards electronics on flexible or organic substrates, which are compatible with sputtering techniques.

Acknowledgements

This work was supported by the National Commission for Scientific and Technological Research through the FONDECYT grants 1150652 (RE) and 1171803 (GG), FONDEQUIP grant EQ M140142 (GG) and National Doctoral scholarship 21151515 (RV).

Appendix A. Supplementary data

Supplementary data related to this article can be found at http://dx.doi.org/10.1016/j.vacuum.2018.04.049.

References

[1] C. Tian, S. Huang, Y. Yang, Anatase TiO2 white pigment production from unenriched industrial titanyl sulfate solution via short sulfate process, Dyes Pigments 96 (2013) 609–613 https://doi.org/10.1016/j.dyepig.2012.09.016.

[2] A. Jaroenworaluck, W. Sunsaneeyametha, N. Kosachan, R. Stevens, Characteristics of silica-coated TiO2 and its UV absorption for sunscreen cosmetic applications, Surf. Interface Anal. 38 (2006) 473–477, http://dx.doi.org/10.1002/sia.2313.

[3] X. Chen, S.S. Mao, X. Chen, S.S. Mao, Titanium dioxide Nanomaterials ;: synthesis, properties, modifications and applications, Chem. Rev. 107 (2007) 2891–2959, http://dx.doi.org/10.1021/cr0500535.

[4] X. Zhang, H. Cui, M. Humayun, Y. Qu, N. Fan, X. Sun, Exceptional performance of photoelectrochemical water oxidation of single-crystal rutile TiO 2 nanorods dependent on the hole trapping of modified chloride, Nat. Publ. Gr. (2016) 1–8, http://dx.doi.org/10.1038/srep21430.

[5] S. Ge, H. Xu, W. Wang, R. Cao, Y. Wu, W. Xu, The improvement of open circuit voltage by the sputtered TiO 2 layer for ef fi cient perovskite solar cell, Vaccum 128 (2016) 91–98, http://dx.doi.org/10.1016/j.vacuum.2016.03.013.

[6] M. Mazur, D. Wojcieszak, J. Domaradzki, D. Kaczmarek, S. Song, TiO 2/SiO 2 Multilayer as an Antireflective and Protective Coating Deposited by Microwave Assisted Magnetron Sputtering vol. 21, (2013), pp. 233–238, http://dx.doi.org/10.2478/s11772.

[7] B.A. Nejand, S. Sanjabi, V. Ahmadi, The effect of sputtering gas pressure on structure and photocatalytic properties of nanostructured titanium oxide self-cleaning thin film, Vacuum 85 (2010) 400–405, http://dx.doi.org/10.1016/j.vacuum.2010.08.001.

[8] H. Zhang, J.F. Banfield, Structural characteristics and mechanical and thermodynamic properties of nanocrystalline TiO2, Chem. Rev. 114 (2014) 9613–9644, http://dx.doi.org/10.1021/cr500072j.

[9] D. Eder, R. Kramer, Stoichiometry of “titanium suboxide” Part 2. Electric properties, Phys. Chem. Chem. Phys. 5 (2003) 1314–1319, http://dx.doi.org/10.1039/B210004E.

[10] J. Yao, J. Shao, H. He, Z. Fan, Optical and electrical properties of TiOx thin films deposited by electron beam evaporation, Vacuum 81 (2007) 1023–1028 https://doi.org/10.1016/j.vacuum.2006.11.002.

[11] S. Siracusano, V. Baglio, C. D'Urso, V. Antonucci, A.S. Aricò, Preparation and characterization of titanium suboxides as conductive supports of IrO2 electrocatalysts for application in SPE electrolysers, Electrochim. Acta 54 (2009) 6292–6299 https://doi.org/10.1016/j.electacta.2009.05.094.

[12] N. He, C. Qin, R. Wang, S. Ma, Y. Wang, T. Qi, Electro-catalysis of carbon black or titanium sub-oxide supported Pd-Gd towards formic acid electro-oxidation, RSC Adv. 6 (2016) 68989–68996, http://dx.doi.org/10.1039/C6RA13097F.

[13] F.C. Walsh, R.G.A. Wills, The continuing development of Magnéli phase titanium sub-oxides and Ebonex electrodes, Electrochim. Acta 55 (2010) 6342–6351, http://dx.doi.org/10.1016/j.electacta.2010.05.011.

[14] B. Xu, H.Y. Sohn, Y. Mohassab, Y. Lan, Structures, preparation and applications of titanium suboxides, RSC Adv. 6 (2016) 79706–79722, http://dx.doi.org/10.1039/C6RA14507H.

[15] S. Andersson, B. Collén, U. Kuylenstierna, A. Magnéli, Phase analysis studies on the titanium-oxygen system, Acta Chem. Scand. 11 (1957) 1641–1652, http://dx.doi.org/10.3891/acta.chem.scand.11-1641.

[16] V. Schöllmann, J. Johansson, K. Andersson, D.B. Haviland, Coulomb blockade effects in anodically oxidized titanium wires, J. Appl. Phys. 88 (2000) 6549–6553, http://dx.doi.org/10.1063/1.1323522.

[17] T. Nguyen, J. He, Preparation of titanium monoxide nanopowder by low-energy wet ball-milling, Adv. Powder Technol. 27 (2016) 1868–1873, http://dx.doi.org/10.1016/j.apt.2016.04.022.

[18] T.T.N. Nguyen, Y.H. Chen, J.L. He, Preparation of inkjet-printed titanium monoxide as p-type absorber layer for photovoltaic purposes, Thin Solid Films 572 (2014) 8–14, http://dx.doi.org/10.1016/j.tsf.2014.09.054.

[19] N. Okinaka, T. Akiyama, Thermoelectric properties of nonstoichiometric TiO as a promising oxide material for high-temperature thermoelectric conversion, Int. Conf. Thermoelectr. ICT, Proc. 2005 (2005) 34–37, http://dx.doi.org/10.1109/ICT.2005.1519880.

[20] H. Fan, M. Wang, Z. Yang, X. Ren, M. Yin, S. Liu, Optical and electrical properties of high-quality Ti2O3 epitaxial film grown on sapphire substrate, Appl. Phys. A Mater. Sci. Process 122 (2016) 1–6, http://dx.doi.org/10.1007/s00339-016-0415-y.

[21] J. Wang, Y. Li, L. Deng, N. Wei, Y. Weng, S. Dong, D. Qi, J. Qiu, X. Chen, T. Wu, High-Performance photothermal conversion of narrow-bandgap Ti $_2$ O $_3$ nanoparticles, Adv. Mater. (2016) 1–6, http://dx.doi.org/10.1002/adma.201603730.

[22] Z. Cao, W. Xie, I.H. Jung, G. Du, Z. Qiao, Critical evaluation and thermodynamic optimization of the Ti-C-O system and its applications to carbothermic TiO_2 reduction process, Metall. Mater. Trans. B Process Metall. Mater. Process. Sci. 46 (2015) 1782–1801, http://dx.doi.org/10.1007/s11663-015-0344-8.

[23] F. Amano, M. Nakata, High-temperature calcination and hydrogen reduction of rutile TiO2: a method to improve the photocatalytic activity for water oxidation, Appl. Catal. B Environ. 158–159 (2014) 202–208, http://dx.doi.org/10.1016/j.apcatb.2014.04.025.

[24] A.A. Gusev, E.G. Avvakumov, À. Zh, Conducting Ceramic Anodes Based on Titanium Oxides, (n.d.) 313–318.

[25] S. Berg, T. Larsson, C. Nender, H. Blom, Predicting thin-film stoichiometry in reactive sputtering, J. Appl. Phys. 63 (1988) 887–891, http://dx.doi.org/10.1063/1.340030.

[26] J. Musil, P. Baroch, J. Vlček, K.H. Nam, J.G. Han, Reactive magnetron sputtering of thin films: present status and trends, Thin Solid Films 475 (2005) 208–218 https://doi.org/10.1016/j.tsf.2004.07.041.

[27] S. Berg, T. Nyberg, Fundamental understanding and modeling of reactive sputtering processes, Thin Solid Films 476 (2005) 215–230 https://doi.org/10.1016/j.tsf.2004.10.051.

[28] D. Severin, O. Kappertz, T. Kubart, T. Nyberg, S. Berg, A. Pflug, M. Siemers, M. Wuttig, Process stabilization and increase of the deposition rate in reactive sputtering of metal oxides and oxynitrides, Appl. Phys. Lett. 88 (2006) 161504, http://dx.doi.org/10.1063/1.2196048.

[29] D. Depla, S. Heirwegh, S. Mahieu, R. De Gryse, D.D., S.H., S.M., R. De Gryse, Towards a more complete model for reactive magnetron sputtering, J. Phys. D Appl. Phys. 40 (2007) 1957, http://dx.doi.org/10.1088/0022-3727/40/7/019.

[30] S. Berg, E. Särhammar, T. Nyberg, Upgrading the “ Berg-model ” for reactive sputtering processes, Thin Solid Films 565 (2014) 186–192, http://dx.doi.org/10.1016/j.tsf.2014.02.063.

[31] M.H. Suhail, G.M. Rao, S. Mohan, Dc reactive magnetron sputtering of titanium-structural and optical characterization of TiO2 films, J. Appl. Phys. 71 (1992) 1421–1427, http://dx.doi.org/10.1063/1.351264.

[32] R. Pandian, G. Natarajan, S. Rajagopalan, M. Kamruddin, A.K. Tyagi, On the phase formation of titanium oxide thin films deposited by reactive DC magnetron sputtering: influence of oxygen partial pressure and nitrogen doping, Appl. Phys. a 116 (2014) 1905–1913, http://dx.doi.org/10.1007/s00339-014-8351-1.

[33] M. Horprathum, P. Eiamchai, P. Chindaudom, A. Pokaipisit, P. Limsuwan, Oxygen partial pressure dependence of the properties of TiO2 thin films deposited by DC reactive magnetron sputtering, Proc. Eng. 32 (2012) 676–682, http://dx.doi.org/10.1016/j.proeng.2012.01.1326.

[34] D. Rafieian, W. Ogieglo, T. Savenije, R.G.H. Lammertink, Controlled formation of anatase and rutile TiO2 thin films by reactive magnetron sputtering, AIP Adv. 5 (2015) 97168, http://dx.doi.org/10.1063/1.4931925.

[35] A. Amin, D. Köhl, M. Wuttig, The role of energetic ion bombardment during growth of TiO $_2$ thin films by reactive sputtering, J. Phys. D Appl. Phys. 43 (2010) 405303, http://dx.doi.org/10.1088/0022-3727/43/40/405303.

[36] B. Wang, S. Wei, L. Guo, Y. Wang, Y. Liang, B. Xu, F. Pan, A. Tang, X. Chen, Effect of deposition parameters on properties of TiO2films deposited by reactive magnetron sputtering, Ceram. Int. 43 (2017) 10991–10998, http://dx.doi.org/10.1016/j.ceramint.2017.05.139.

[37] K.G. Geraghty, Kinetics of the reactive sputter deposition of titanium oxides, J. Electrochem. Soc. 123 (1976) 1201–1207, http://dx.doi.org/10.1149/1.2133036.

[38] F. Lapostolle, A. Billard, J. von Stebut, Structure/mechanical properties relationship of titanium–oxygen coatings reactively sputter-deposited, Surf. Coating. Technol. 135 (2000) 1–7 https://doi.org/10.1016/S0257-8972(00)00721-0.

[39] G.S. Chen, C.C. Lee, H. Niu, W. Huang, R. Jann, T. Schütte, Sputter deposition of titanium monoxide and dioxide thin films with controlled properties using optical emission spectroscopy, Thin Solid Films 516 (2008) 8473–8478, http://dx.doi.org/10.1016/j.tsf.2008.04.093.

[40] W.C. Peng, Y.H. Chen, J.Y. Chen, J.L. He, D.S. Wuu, High power impulse magnetron sputtered p-type γ-titanium monoxide films: effects of substrate bias and post-annealing on microstructure characteristics and optoelectrical properties, Mater. Sci. Semicond. Process. 61 (2017) 85–92, http://dx.doi.org/10.1016/j.mssp.2017.01.005.

[41] CS = k/FWHM/cosH; K: 0.15418 Nm (X-ray Wavelength), FWHM: Full-width-at-half-maximum of the Bragg Reflection, H: Bragg Angle, (n.d.).

[42] C.U. Pinnow, I. Kasko, C. Dehm, B. Jobst, M. Seibt, U. Geyer, Preparation and properties of dc-sputtered IrO[sub 2] and Ir thin films for oxygen barrier applications in advanced memory technology, J. Vac. Sci. Technol. B Microelectron. Nanom. Struct. 19 (2001) 1857, http://dx.doi.org/10.1116/1.1401750.

[43] D. Guerin, S.I. Shah, Reactive-sputtering of titanium oxide thin films, J. Vac. Sci. Technol. A Vac. Surfaces Film 15 (1997) 712–715, http://dx.doi.org/10.1116/1.580807.

[44] Bo Holmberg, Disorder and order in solid solutions of oxygen in alpha-titanium, Acta Chem. Scand. 16 (1962) 1245–1250, http://dx.doi.org/10.3891/acta.chem.scand.16-1245.

[45] J.A. Thornton, The microstructure of sputter-deposited coatings, J. Vac. Sci. Technol. A Vac. Surfaces, Film 4 (1986) 3059–3065, http://dx.doi.org/10.1116/1.573628.

[46] P. Kern, J. Michler, Local electron beam induced reduction and crystallization in electrochemically deposited amorphous TiO2 films, MRS Proc. 950 (2007), http://dx.doi.org/10.1557/PROC-0950-D15-18.

[47] C. Ma, G.R. Rossman, Tistarite, ti203, a new refractory mineral from the allende meteorite, Am. Mineral. 94 (2009) 841–844, http://dx.doi.org/10.2138/am.2009.3203.

[48] M. Sobaszek, K. Siuzdak, M. Sawczak, J. Ryl, R. Bogdanowicz, Fabrication and characterization of composite TiO2 nanotubes/boron-doped diamond electrodes towards enhanced supercapacitors, Thin Solid Films 601 (2016) 35–40, http://dx.doi.org/10.1016/j.tsf.2015.09.073.

[49] G.A. Tompsett, G.A. Bowmaker, R.P. Cooney, J.B. Metson, K.A. Rodgers, J.M. Seakins, The Raman spectrum of brookite, TiO2, J. Raman Spectrosc. 26 (1995) 57–62.

[50] V.H. Castrejon-Sanchez, E. Camps, M. Camacho-Lopez, C. Enrique, Quantification of phase content in TiO2 thin films by Raman spectroscopy, Superf. Y Vacio 27 (2014) 88–92.

[51] C. Guillén, J. Herrero, TiO2 coatings obtained by reactive sputtering at room temperature: physical properties as a function of the sputtering pressure and film thickness, Thin Solid Films 636 (2017) 193–199, http://dx.doi.org/10.1016/j.tsf.2017.05.048.